# Manifold Learning of Nonlinear Airfoil Aerodynamics with Dimensionality Reduction

Vasudevan, S.; De Breuker, R.; Wang, Xuerui

**DOI**
10.2514/6.2023-1199

**Publication date**
2023

**Document Version**
Final published version

**Published in**
AIAA SciTech Forum 2023

AIAA SciTech Forum
23-27 January 2023, National Harbor, MD & Online
AIAA SCITECH 2023 Forum

10.2514/6.2023-1199

# Manifold Learning of Nonlinear Airfoil Aerodynamics with Dimensionality Reduction

Srikanth Vasudevan*, Roeland De Breuker†, Xuerui Wang‡
*Delft University of Technology, Delft, The Netherlands*

**This paper aims to explore the advantages offered by machine learning (ML) for dimensionality reduction of nonlinear transonic aerodynamics. Three ML techniques are evaluated in terms of their ability to generate interpretable low-dimensional manifolds of the transient pressure distributions over a NACA4412 airfoil equipped with a flap. These ML techniques are Kernel Principle Component Analysis (kPCA), Locally Linear Embedding (LLE), and t-distributed Stochastic Neighbourhood Embedding (t-SNE). Initial investigations are also carried out to evaluate the performance of Artificial Neural Networks (ANNs). Three transient aerodynamic test cases are evaluated. First, a static aerodynamic transient analysis. Second, pitching and heaving airfoils in terms of prescribed sinusoidal displacements. Lastly, the airfoil geometry is adapted to include a flap under sinusoidal actuation. The snapshots forming the ground truth are obtained from unsteady CFD simulations. The preliminary results of this study reveal that patterns exist in low-dimensional nonlinear manifolds. Furthermore, unsupervised learning techniques are seen to outperform supervised neural networks in terms of both training cost and reconstruction accuracy. Promising reconstruction capabilities are observed with unsupervised learning.**

## I. Nomenclature

| | | |
|---|---|---|
| $P$ | = | Pressure, Pa |
| $X$ | = | Chord, m |
| $h$ | = | Height, m |
| $t$ | = | Time, s |
| $\alpha$ | = | Angle of attack, degrees |
| $\beta$ | = | Angle of flap, degrees |
| $\pm\Delta$ | = | Incremental quantity, degrees |
| $\omega$ | = | Frequency of sinusoidal input, Hz |
| $\Psi_{\kappa 1}$ | = | Latent dimension 1 |
| $\Psi_{\kappa 2}$ | = | Latent dimension 2 |
| $\Psi_{\kappa 3}$ | = | Latent dimension 3 |
| $C_l$ | = | Coefficient of lift |
| $C_d$ | = | Coefficient of drag |
| $C_p$ | = | Coefficient of pressure |
| $M$ | = | Mach number |
| $Re$ | = | Reynolds number |

*Ph.D. Candidate, Aerospace Structures and Materials, Faculty of Aerospace Engineering, Delft University of Technology, S.Vasudevan@tudelft.nl, Student member AIAA.

†Associate Professor, Aerospace Structures and Materials, Faculty of Aerospace Engineering, Delft University of Technology, R.DeBreuker@tudelft.nl, Associate Fellow AIAA.

‡Assistant Professor, Aerospace Structures and Materials & Control and Operations, Faculty of Aerospace Engineering, Delft University of Technology, X.Wang-6@tudelft.nl, Member AIAA.

## II. Introduction

With computing power growing at an exponential rate, the formulation of "digital twins" is crucial in attaining the ambitious sustainability goals of the next decade. Digitalisation offers several benefits such as cost-effective simulations, non-destructive virtual testings, predictive maintenance and condition monitoring. However, one of the major limitations of physics simulations is their reliance on high fidelity solvers such as Computational Fluid Dynamics (CFD) for accurate predictions of complex fluid flows. Furthermore, for multidisciplinary fields such as Aeroservoelasticity (ASE), simulating the interactions between structures, aerodynamics and control is crucial [1]. This requires a consistent and efficient transfer of information between models with varying degrees of complexity. In such scenarios, Model Order Reduction (MOR) techniques are typically employed to reduce the complexity of the simulations [1].

Modal analysis as a standard MOR technique has existed in the field of structures for several decades [2]. Proper Orthogonal Decomposition (POD) is commonly employed for simulations involving fluid flows [3–5]. In particular, CFD-based reduced order models (ROMs) have been an active field of research for several decades [6]. As ROMs are seen as surrogate models of a physical system, it begins with snapshots of the systems of interest taken as the ground truth, following which eigenvalue-based subspace projection is performed. Several methods such as Discrete Fourier Transforms (DFT), Dynamic Mode Decomposition (DMDs), multiscale POD (mPOD) exist in literature [7–9]. However, these linear techniques are often described for simple 2D example cases and their performance normally degrade when applied to nonlinear systems [10].

The aforementioned linear methods can be extended to generate "adaptive" Nonlinear Reduced Order Models (NL-ROMs) via interpolation between local reduced bases [11–14]. The rationale of sparse identification of nonlinear dynamics is to represent the complex dynamics in terms of a few dominant latent coordinates [15]. This, in combination with an exponential increase in trend towards Machine Learning (ML) research has led to the development of Artificial Neural Networks (ANNs) for complex flow physics [16–19]. Moreover, combining the effects of projection-based reductions with sequential dense layers enables superior data compression and dimensionality reduction [16]. General approaches to simulate dynamical systems using ANNs include direct methods (where temporal information is provided as an input) and time-stepper methods (ANNs augmented with numerical time marching schemes) [20]. Physics is often incorporated into the loss function of the training phase to improve the generalisability of a given solution. Finally, to tackle uncertainties in the predictions, often probability and stochasticity are taken into account with the use of a Bayesian framework [20].

In particular, two recent applications towards transonic aerodynamic predictions indicate promising future research directions. Bertrand et al. [21] investigated the performance of ANNs and U-Nets in predicting the transonic flow around the RAE2822 airfoil. These supervised ML techniques were found to predict the transonic pressure distribution over the 2D airfoil with a high degree of accuracy. However, their large training dataset consisted of up to 150,000 steady simulations. Also, the ANNs were incapable of accurately predicting the linear subsonic regime thus making them inherently dependent on the large training datasets. A more recent work by Vladyslav et al. [22] improved upon these limitations with a major advantage of a temporal prediction using previous time steps. The training dataset was drastically reduced here by using the approach of Averaged Pseudo-Random Signal (APRS) that typically excites a frequency range of interest. The Encoder-Decoder and the U-Net architectures were seen to accurately predict the temporal evolutions for a range of reduced-order frequency excitations [22].

However, although prediction accuracies were high in these simulations, grey box (non-intrusive) approaches were utilised without any studies on the patterns that could exist in the low-dimensional manifold. Identifying these patterns is crucial for sparse representation of complex nonlinear and multi-physical systems. This can reduce the computational requirements by several orders of magnitude. Although ANNs are known for their predictive prowess, they are often not physically interpretable. Using ANNs in the form of deep autoencoders to predict within the realms of these identified manifolds could aid in better data compression with added physical intuition of the system [16]. Furthermore, most aerodynamic ROMs in the literature do not model the flap system. Capturing the influence of control surfaces is crucial for aeroservoelastic applications such as transonic flutter suppression.

This paper aims to build reduced-order transonic aerodynamic models by identifying low-dimensional manifolds where patterns could exist in highly nonlinear aerodynamic systems. To this end, a 2D airfoil is first used in a static unsteady

test case. Next, the evolution of aerodynamic loads due to prescribed pitching and plunging motion is analysed. Finally, a prescribed flap actuation simulation is carried out to analyse the flap model.

## III. Methodology

This section briefly describes the numerical setup and the mathematical procedures that are utilised in this paper. First, the geometry and settings used for CFD simulations are presented in section III.A. Subsequent sections provide the mathematical descriptions of the reduction algorithms evaluated in this paper. For ease of comparison, the classical linear POD approach and the related machine-learning methods III.B and III.C are presented sequentially.

### A. Geometry and Computational Domain Definition

Figure 1 illustrates the geometry and preliminary test cases evaluated. Figure 2 along with table 1 describe the computational domain used for generating the high fidelity snapshots.

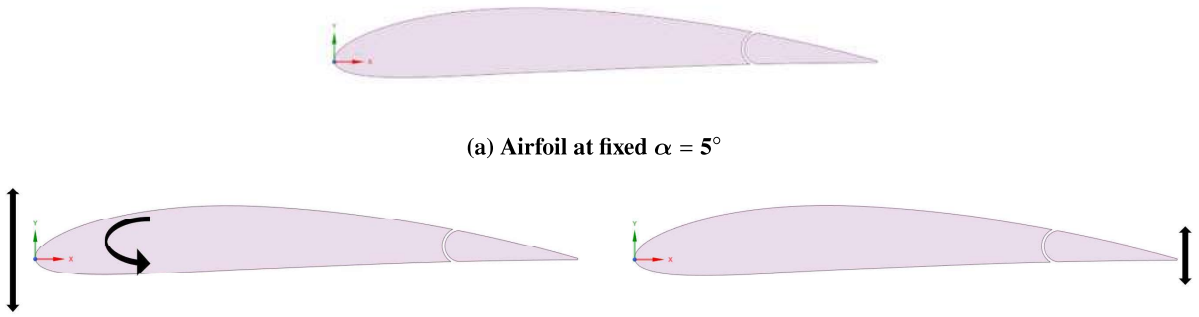

**(a) Airfoil at fixed $\alpha = 5°$**

**(b) Pitching and heaving airfoil at $\omega = 5$ Hz**

**(c) Flap actuation at $\omega = 5$ Hz**

**Fig. 1 Preliminary test cases on a NACA 4412 airfoil equipped with a flap.**

In this paper, ANSYS Fluent 21R2 was used for the unsteady Reynolds-Average Navier Stokes (uRANS) simulations. The governing partial differential equations are discretised using finite volume method that results in an expensive high-dimensional system (set of ordinary differential equations) that is solved using time-stepping methods. We use the 1-equation Spallart-Allmaras (SA) turbulence model due to its suitability for external flows over airfoils [23]. Three simulation scenarios are studied in this work:

1) The unsteady flow around a NACA4412 airfoil with a static angle of attack $\alpha = 5$ deg at $M = 0.85$.
2) The airfoil is prescribed with 5 pitch and heave oscillations with frequencies $\omega$ = 0.5Hz, 1Hz, 2Hz, 10Hz, 20Hz about the mid-chord.
3) The airfoil is equipped with a trailing edge flap (0.2c, i.e 20% of chord), to which the above oscillations are prescribed, simulating flap actuation at varying frequencies.

Each simulation is carried out for $t = 5s/10s$, with a timestep of $\Delta t = 0.005s/0.01s$. The choice of these frequencies is based on the parameter reduced frequency $k$ (where $k = \omega b/U_\infty$, $\omega$ is angular frequency in radians/sec, b is the semi-chord in m and $U_\infty$ is the freestream velocity in m/s) which take the values $k = 0.00215, 0, 0107, 0.0215, 0.107, 0.215$. These k values are of interest to the aeroelastician as a measure of flow unsteadiness. Thus, this study consists of 16 snapshots in total which form the ground truth for all results discussed in this paper. The spatial discretisation of the complete flow field leads to $n_x = 5.53 \times 10^5$ degrees-of-freedom, which are the locations at which pressures are evaluated.

**Table 1 CFD Simulation Settings.**

| Property | Definition |
|---|---|
| Bounding box | 15X × 10X (X is the airfoil chord) |
| Mesh domain | Mapped face meshing with $5.53 \times 10^5$ nodes |
| Airfoil geometry | NACA4412, 1 m chord, $\alpha = 5°$ |
| Flow settings | Spalart Allmaras RANS model, Mach 0.85 |

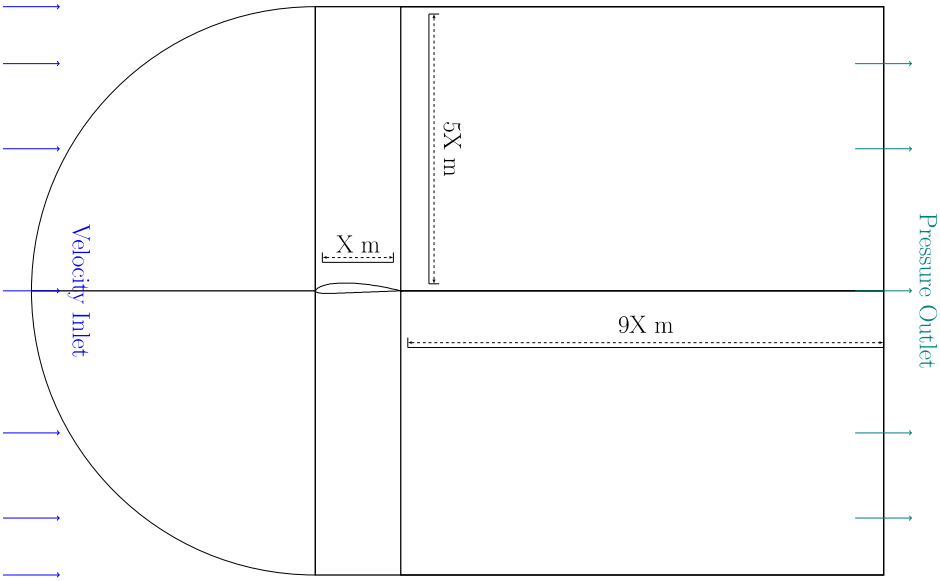


**Fig. 2 CFD domain definition for structured face meshing.**

### B. Proper Orthogonal Decomposition

The Proper Orthogonal Decomposition is a physics-based parametrisation of a given field variable, u and can be expressed as a separation of variables as follows [24]:

$$\hat{\boldsymbol{u}}(\boldsymbol{t}) = \Sigma_{k=1}^{n} \boldsymbol{v_k} \alpha_k(t)$$

where $\hat{\boldsymbol{u}}$ is the approximate solution of the field variable of interest u, $\boldsymbol{v_k}$ represents a set of spatial modes that form the POD basis and $\boldsymbol{\alpha_k}$ are the temporal coefficients of the basis.
In practice, the POD basis is computed using the method of snapshots, where a Singular Value Decomposition (SVD) of the field variable matrix $\boldsymbol{U}$ gives us the following:

$$\boldsymbol{U} = \boldsymbol{V \Sigma W^T}$$

The POD basis vectors are then the first r columns of $\boldsymbol{V}$, $\boldsymbol{V_r} = [\boldsymbol{v_1}, \boldsymbol{v_2}, ...\boldsymbol{v_r}]$ and are orthonormal. The singular matrix $\boldsymbol{\Sigma}$ is a diagonal matrix of ordered singular values such that the r-rank truncation results in $\boldsymbol{V_r}$ corresponding to r highest singular values.

### C. ML Algorithms for Dimensionality Reduction

This section briefly describes the main mathematical formulations behind the data-driven algorithms used in the current work. Three algorithms are presented. Additionally, the autoencoder architecture is briefly described in the subsequent section separately.

#### *1. Kernel Principle Component Analysis (kPCA)*

The kernel method can be seen as extension of the POD procedure described above with a nonlinear projection step. Given a nonlinear function $\boldsymbol{\Phi(x)} : \mathbb{R}^d \mapsto \mathbb{R}^n$ (n > d), a kernel is defined as [25]:

$$K(x, y) = \boldsymbol{\Phi(x)}^T \boldsymbol{\Phi(y)}$$

Projecting a point from the kernelised high-dimensional data onto one of the principle coordinates $\boldsymbol{V_k} \in \boldsymbol{V_r}$, we get

$$\boldsymbol{V_k}^T \boldsymbol{\Phi(x_i)} = \Sigma_i (a_i^k \boldsymbol{\Phi(x)})^T \boldsymbol{\Phi(x)}$$

Now solving the eigenvector equation for $a_i^k$ gives us the solution,

$$N\lambda a = Ka$$

N is the dimension of the data, $\lambda$ is the eigenvalue of K.

#### *2. Locally Linear Embedding (LLE)*

Locally Linear Embedding attempts to reduce the dimensionality of a given dataset by preserving a "nearest neighbour" metric around the individual data points. This is done by first performing a k-nearest neighbour (kNN) search in the high dimensional space. A weight matrix is then built using this kNN search, which is mapped onto the low-dimensional space. Mathematically, a reconstruction cost function, $\boldsymbol{\xi(W)}$, based on L2 norm can be defined as follows [26]:

$$\boldsymbol{\xi(W)} = \Sigma_i |\boldsymbol{X}_i - \Sigma_j \boldsymbol{W}_{ij} \boldsymbol{X}_j|^2$$

where $\boldsymbol{W}_{ij}$ is the weight matrix constructed based on the number of nearest neighbours. $\boldsymbol{X}_i \in \mathbb{R}^n$ is the high-dimensional data. These weights are used in the embedding cost function, $\boldsymbol{\Phi(Y)}$, defined as :

$$\boldsymbol{\Phi(Y)} = \Sigma_i |\boldsymbol{Y}_i - \Sigma_j \boldsymbol{W}_{ij} \boldsymbol{Y}_j|^2$$

where $\boldsymbol{Y}_i \in \mathbb{R}^m (m << n)$ is the obtained low-dimensional data.

#### *3. t-distributed Stochastic Nonlinear Embedding (t-SNE)*

Similar to the approach of maintaining a measure of euclidean distance in an LLE algorithm described above, t-SNE embeds a similarity measure between two points in the high-dimensional data. This similarity measure is a conditional probability function defined between two points as:

$$p_{j|i} = \frac{exp(-||\boldsymbol{X}_i - \boldsymbol{X}_j||^2 / 2\sigma_i^2)}{\Sigma_{k \neq i} exp(-||\boldsymbol{X}_i - \boldsymbol{X}_k||^2 / 2\sigma_i^2)}$$

The similarity in the high dimensional dataset is then defined as

$$p_{ij} = \frac{p_{j|i} + p_{j|i}}{2N}$$

Now, this operation is performed for the low dimensional map,

$$q_{j|i} = \frac{exp(-||\boldsymbol{Y}_i - \boldsymbol{Y}_j||^2 / 2\sigma_i^2)}{\Sigma_{k \neq i} exp(-||\boldsymbol{Y}_i - \boldsymbol{Y}_k||^2 / 2\sigma_i^2)}$$

$$q_{ij} = \frac{q_{j|i} + q_{j|i}}{2N}$$

where $p_{j|i}$ and $q_{j|i}$ are the PDFs, $p_{ij}$ and $q_{ij}$ are the similarity metrics based on the PDFs, $\boldsymbol{X}_i \in \mathbb{R}^n$ and $\boldsymbol{Y}_i \in \mathbb{R}^m$ are the high and reduced dimensional data respectively.

Finally, the t-SNE algorithm minimises the Kullback-Leiber (KL) divergence using gradient descent.

$$KL = \Sigma p_{ij} log \frac{p_{ij}}{q_{ij}}$$

### D. Deep Autoencoder Architecture

An autoencoder is a Neural Network architecture that aims to identify a nonlinear map $f : x \mapsto \hat{x}$, where $x, \hat{x} \in \mathbb{R}^n$ using 3 parts which can be identified as: the encoder, the bottle-neck and the decoder. Mathematically, the nonlinear function can be defined as follows:

$$f : x \mapsto \psi_E \cdot \phi_D(x)$$

where the encoder transformation $\psi_E$ is given by,

$$\psi_E : x \mapsto z$$

with $x \in \mathbb{R}^n, z \in \mathbb{R}^d$ (representing the bottle-neck), $d << n$ and the decoder transformation $\phi_D$ given by,

$$\phi_D : z \mapsto \hat{x}$$

Both the encoder and the decoder consist of several fully connected layers whose weights and biases are learned via the training operation using Stochastic Gradient Descent (SGD).

## IV. Results and Discussions

The simulation results from the three test cases, illustrated in Figure 1 are discussed in this section. Three nonlinear dimensionality reduction algorithms from III are tested for their suitability in building ROMs for nonlinear fluid flow problems involving shockwaves and flow separation. Firstly, results from high fidelity simulations are presented in section IV.A. Next, performance of the data-driven reduction algorithms in the context of nonlinear aerodynamics is discussed in section IV.B.

### A. Full Order Model Fluid Flow Analysis

The setup of the fluid problem was described in section III.A. Here, the results obtained from a total of 16 uRANS CFD simulations over a NACA4412 airfoil at Mach 0.85 ($U_\infty$ = 291.55 m/s) are presented.

Figure 3 presents the validation of the airfoil simulation model used in this work. To begin with, verification is carried out for a steady, low-subsonic NACA4412 airfoil at $\alpha$ = 13.87 deg, $M$ = 0.09, $Re$ = 1.52$E$6 against standard Spallart Allmaras (SA) and $k-\omega$ Shear Stress Transport (SST) evaluations [27]. Also, the model is validated against experimental results at this configuration as shown in figure 3a. The lift coefficient converged to a value $C_l$ = 1.72 as predicted in literature [28]. Figures 3b and 3c illustrate the transonic, unsteady, transient lift and drag histories and chordwise pressure distribution over a NACA4412 airfoil at $\alpha$ = 5 deg, M = 0.85 ($U_\infty$ = 291.55 m/s) respectively. As the obtained time history plots remain bounded over the entire simulation, along with the static validation results from Figure 3a, the transient results are deemed to be valid.

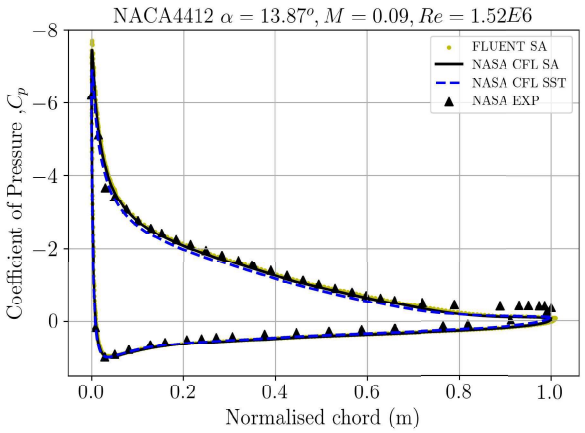


**(a) Validation of simulation for stall angle of NACA4412 at $\alpha$ = 13.87 deg.**

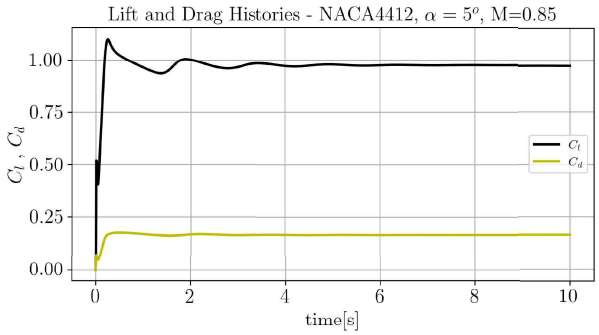


**(b) $C_l$, $C_d$ time history**

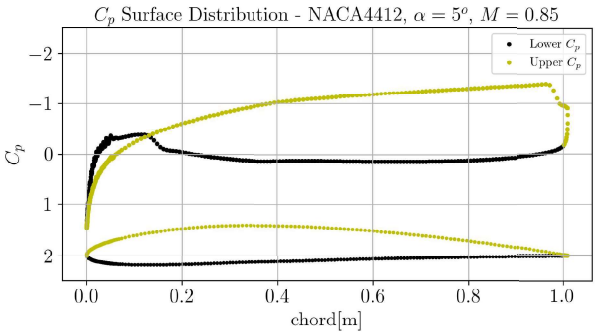


**(c) $C_p$ surface distribution plot**

**Fig. 3 CFD Steady and uRANS simulation of a NACA4412 airfoil (static) at $\alpha$ = 5 deg, $M$ = 0.85.**

Figures 4 and 5 illustrate the lift and drag histories and pressure distributions due to sinusoidal heaving and pitching, respectively. Five frequencies of oscillation are chosen in order to study the effect of reduced frequencies on flow unsteadiness. For the heaving case 4, it is interesting to note that the total unsteady flow is a convolution of the heaving and flow development as a multiple timescales phenomenon. For the sinusoidal pitching motion of the airfoil in Figure 5, the trend in $C_l$ is consistent with Theodorsen aerodynamics, wherein, the slope of $C_l$ vs reduced frequency curve reduces with increasing reduced frequency.

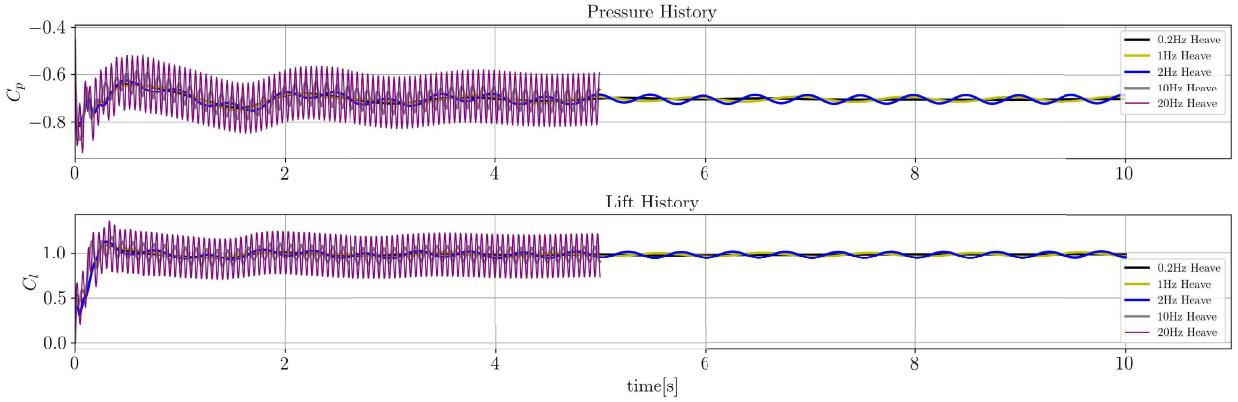


**Fig. 4 CFD uRANS simulation of a NACA4412 airfoil (Heave dynamics) at $H = \pm 0.1m, \alpha_0$ = 5 deg, $M$ = 0.85.**

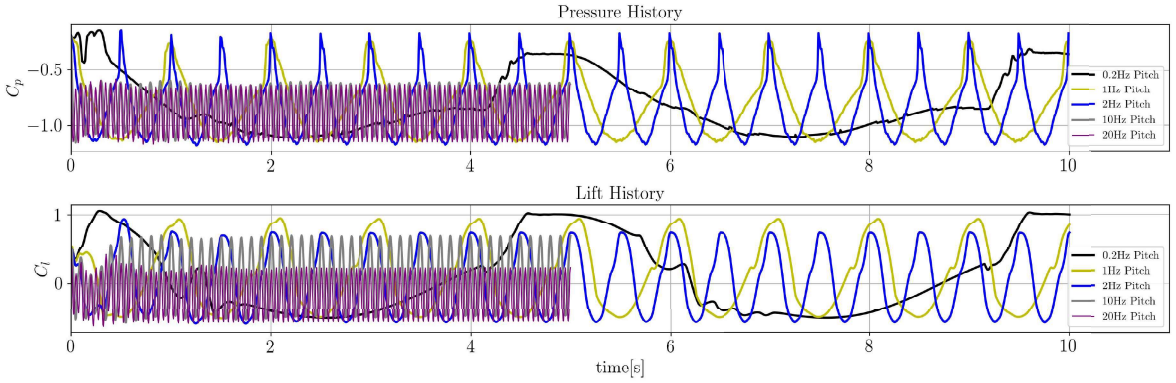


**Fig. 5 CFD uRANS simulation of a NACA4412 airfoil (Pitch dynamics) at $\alpha = \pm 5$ deg, $M = 0.85$.**

Finally, to study the effect of flap actuation on transonic air loads, the airfoil is equipped with a flap at the trailing edge. The above set of oscillatory inputs are now given to the flap hinge-line. The high fidelity simulation results of this test case are illustrated in figure 6. As shown, the simulation of 20Hz actuation seizes to run due to mesh skewness. This will be rectified in future work.

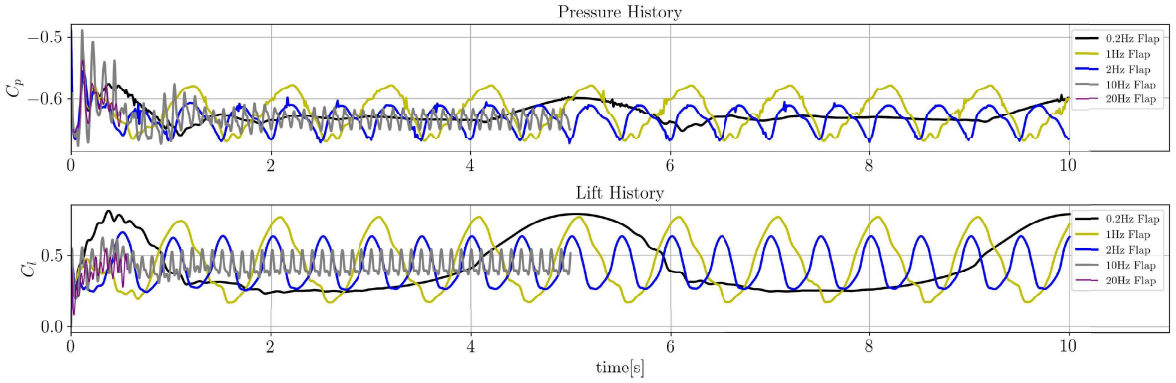


**Fig. 6 CFD uRANS simulation of NACA 4412 (Flap dynamics) at $H = \pm 0.1m, \alpha_0 = 5$ deg, $M = 0.85$.**

### B. Dimensionality Reduction using ML algorithms

The performance of the three machine learning algorithms presented in section III.C are evaluated and compared to the standard POD technique for the each of the test cases presented above. For each algorithm, the reconstruction capabilities, the patterns in the latent manifolds and the computational efficiencies are discussed.

#### *1. Test Case I : Static Aerodynamics*

Figure 7 shows the high-fidelity steady pressure field around the airfoil (Figure 7a ) at t = 10s and it's reconstruction using Proper Orthogonal Decomposition in Figures 7a and 7c.

Comparing the reconstructions and their respective error fields, it is evident that although the linear POD algorithm is capable of reasonably good reconstructions, the error mainly arises along the shock wave region (with a maximum of about 10% in Figure 7c). This is expected as the nature of the solution changes abruptly across the shock wave. The approximation capabilities of the POD recovers after the shock region where it is linear again. Figures 7d and 7e show the advantage of using the Radial Basis Function (RBF) kernels with improvements in the error to about 2.5 % with the kernel-PCA algorithm.

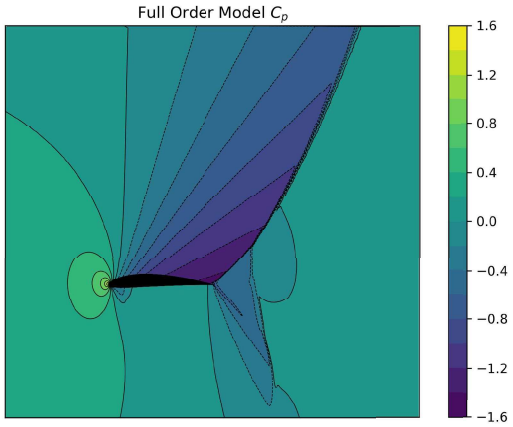


**(a) uRANS CFD Pressure Field**

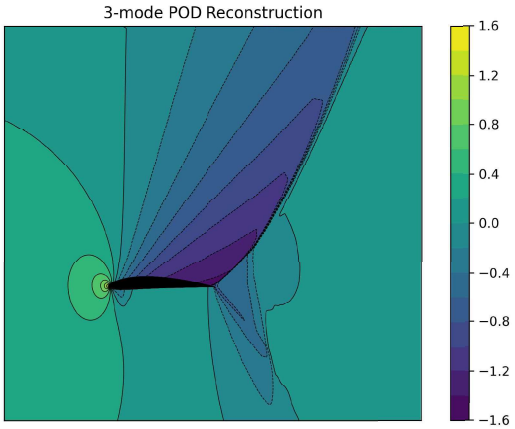


**(b) Linear POD**

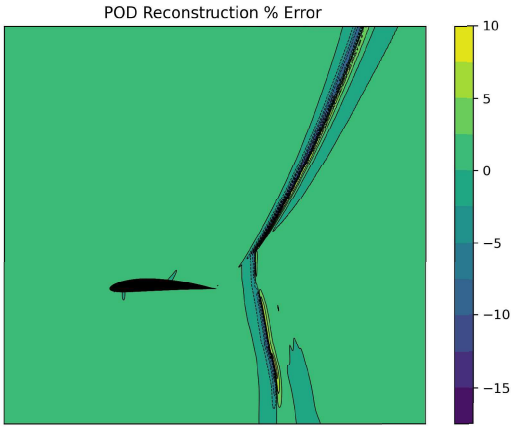


**(c) % Error in POD reconstruction**

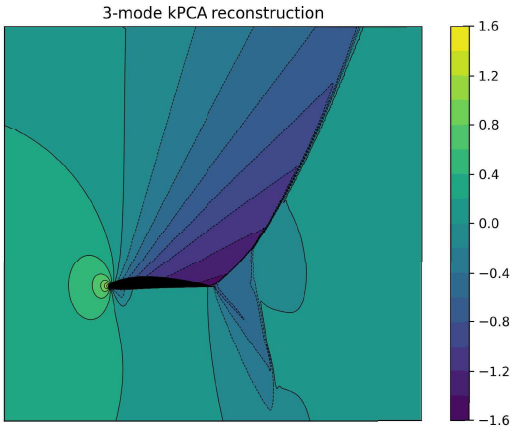


**(d) Nonlinear kernel PCA**

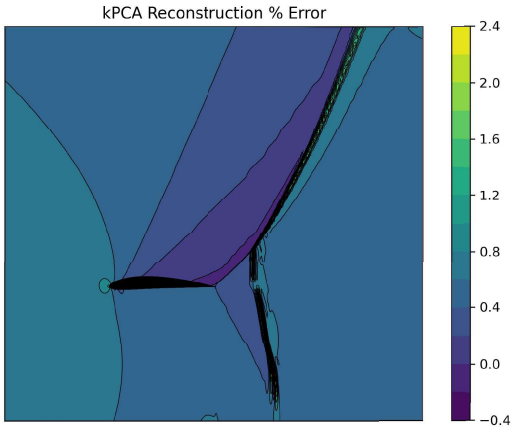


**(e) % Error in kPCA reconstruction**

**Fig. 7 Comparison of FOM pressure field (a) with those reconstructed from latent coordinates using machine learning tools.**

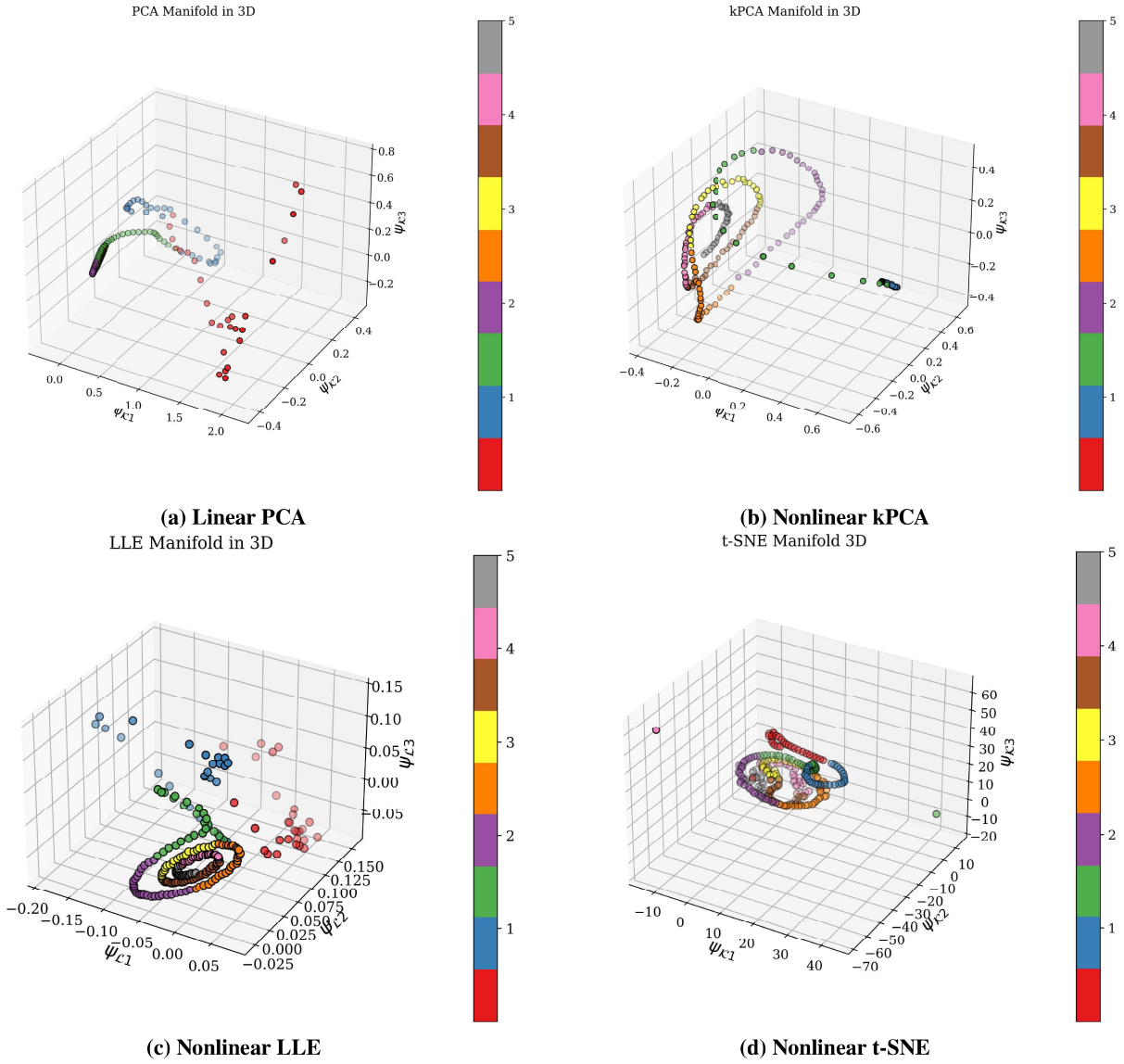


**(a) Linear PCA** **(b) Nonlinear kPCA**

**(c) Nonlinear LLE** **(d) Nonlinear t-SNE**

**Fig. 8 Patterns in the latent manifolds for various machine learning algorithms.**

To better understand the improvement in the above reconstruction, the latent subspaces obtained after nonlinear transformation using various data-driven algorithms are given in Figure 8. With the kernel PCA algorithm, the linear subspace is transformed as shown in Figure 8b. The total pressure distribution over the airfoil forms the data matrix D, with each column vector representing the spatial airfoil data at a given timestep $t_k$. Figure 8 shows the results obtained using the three nonlinear model reduction techniques. The colourbar represents the evolution of the reduced state with respect to time. Thus, in all the following figures, the state of the system transitions from red to gray with time in seconds. $\Psi_{\kappa 1}, \Psi_{\kappa 2}, \Psi_{\kappa 3}$ represent the reduced, latent coordinate system within which we aim to identify the dominant patterns.

The simulation domain was initialised with the inlet velocity of Mach 0.85 at $t = 0$ s. Results from the three dimensionality reduction techniques are shown in Figure 8. Here, the ability of nonlinear reduction to predict dominant patterns in the data is clearly evident as the traditional POD/PCA technique suffers to generate a coherent pattern in figure 8a. Comparing Figures 8b to 8c, the transition towards a fixed attractor is clearly visible with predictable evolution after about 1.6 seconds (green). This is attributed to the initial numerical transitory period where a high degree of randomness exists. The existence of such a pattern in spite of completely different formulations makes these techniques

good candidates for robustness. Techniques such as the t-SNE, see Figure 8d, are not suitable for transient dynamics and were found to be computationally inefficient.

*2. Test Case II : Pitching and Heaving Airfoil Preliminary Analysis*

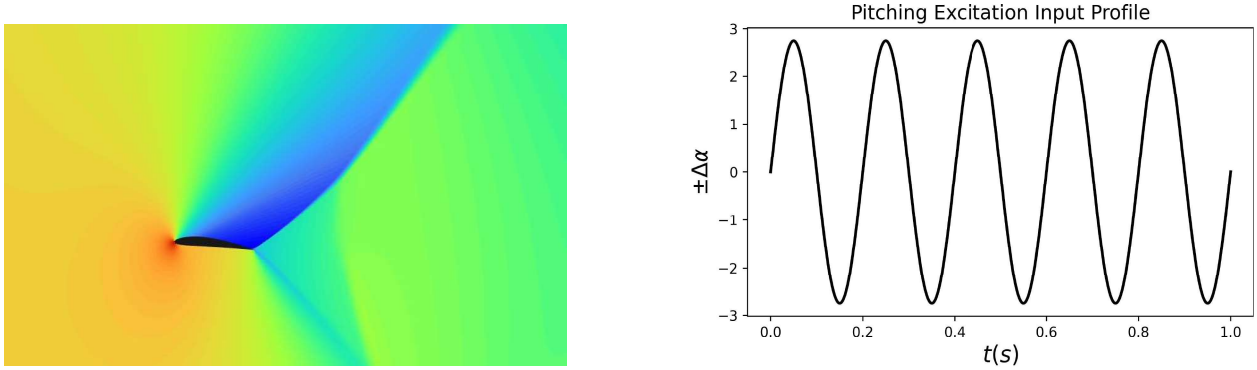


**Fig. 9 Airfoil pitch at $\omega = 5$ Hz.**

Next, the airfoil in pitching and heaving motions are evaluated and the results of high fidelity simulations are shown in Figures 4 and 5. A preliminary simulation was conducted with a prescribed pitching $\pm\Delta\alpha$ with a frequency of 5Hz as shown in Figure 9. In comparison to the previously discussed static case, heaving and pitching airfoil aerodynamic simulations pose additional challenges with moving meshes in a given reference frame. To address this physical change in simulation domain, surface pressure distributions are used in this analysis. The latent manifolds are shown in Figure 10.

It is interesting to note here that similar low dimensional patterns are obtained for this test case using both linear and nonlinear methods. This is attributed to the fact that a pitching profile was prescribed to the system, see Figure 9, which forms the most dominant pattern in the dataset. Firstly, a temporal transition is seen along one dimension. And along the others, an oscillatory trajectory can be observed, especially in the nonlinear methods of kPCA, see Figure 10b, and LLE, see Figure 10c. This way, the nature of the forcing function could potentially be inferred and aids in system parametrisation.

The results obtained from a preliminary heaving airfoil test case are not presented here. From initial observations of the heaving test case, it is hypothesised that the effect of heaving on dominant low-dimensional patterns is not as influential as the airfoil pitching case presented here. The change in effective angle of attack $\pm\Delta\alpha$ due to a given heaving velocity $\dot{h}$ as observed in Figure 4 is still within the linear range of $c_l$ vs $\alpha$.

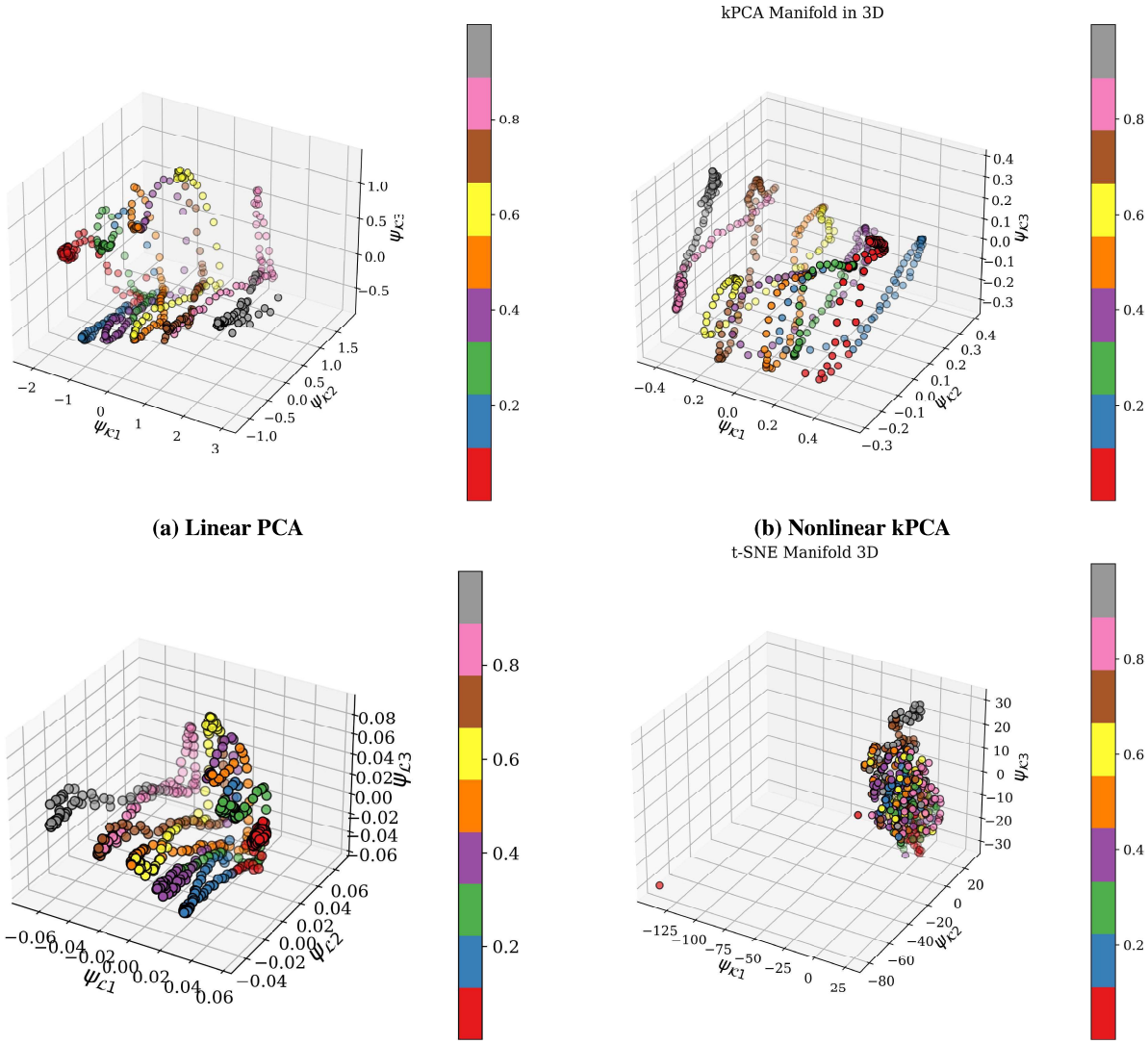


**(a) Linear PCA** **(b) Nonlinear kPCA**

**(c) Nonlinear LLE** **(d) Nonlinear t-SNE**

**Fig. 10 Results from dimensionality reduction of dynamic pitch excitation.**

### *3. Test Case III : Dynamic Flap Actuation*

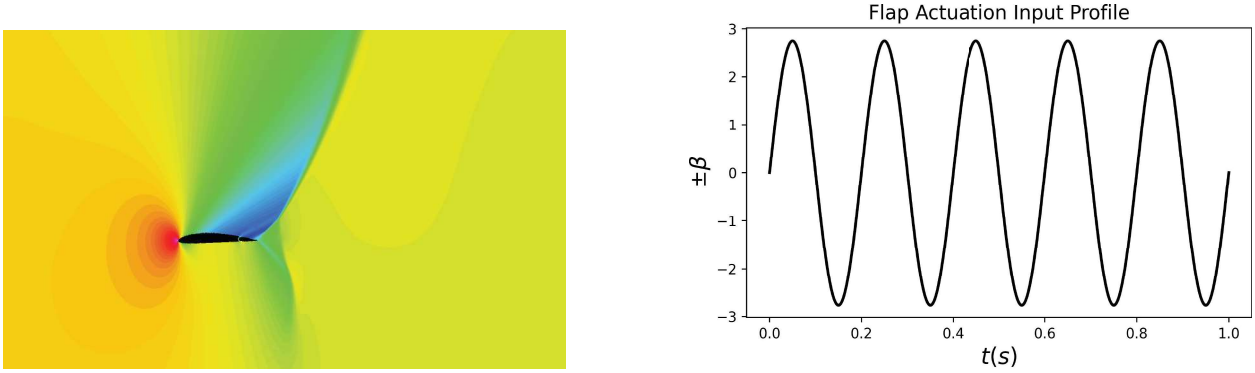


**Fig. 11 Flap Actuation at $\omega$ = 5 Hz.**

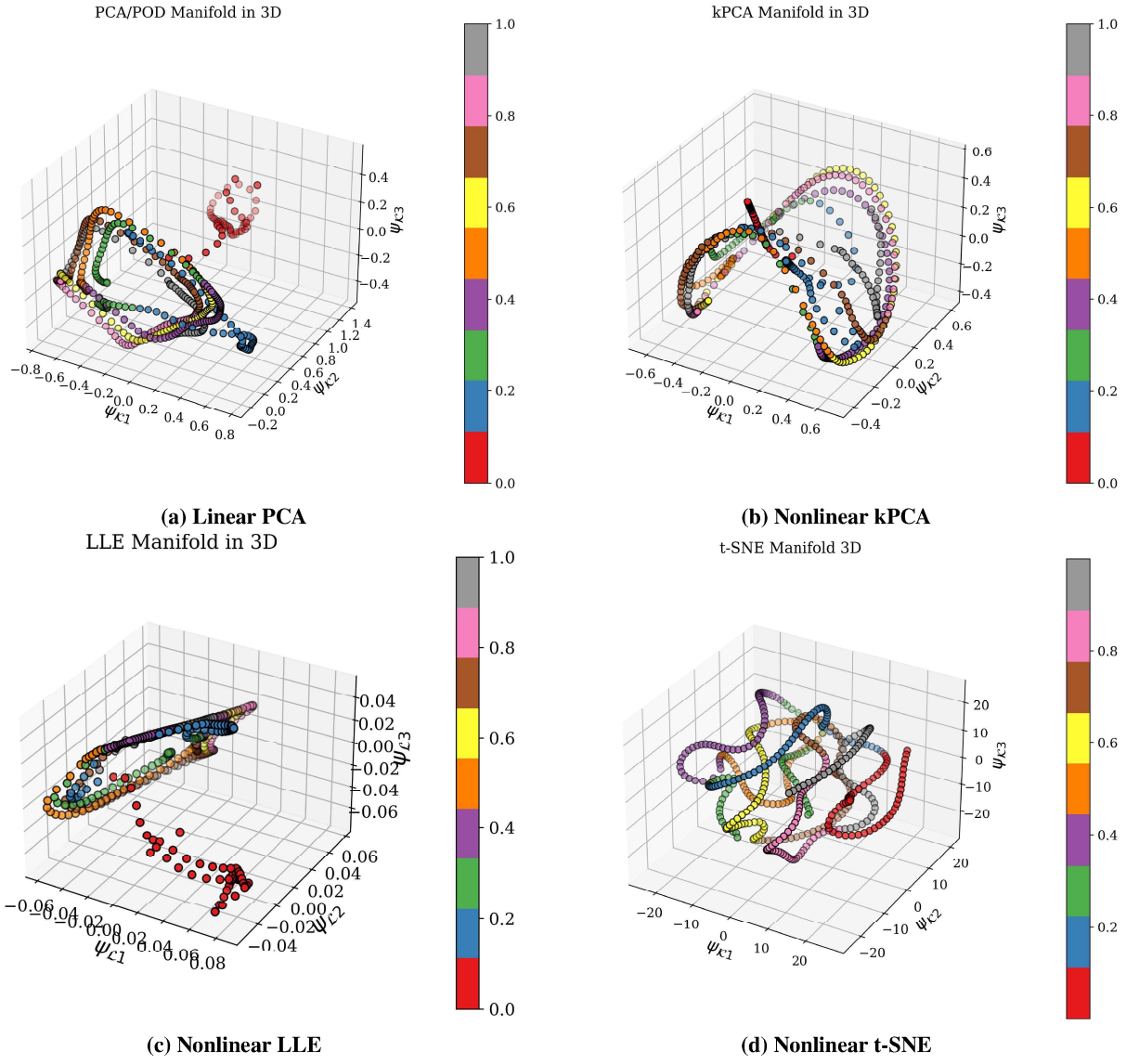


**(a) Linear PCA** **(b) Nonlinear kPCA**

**(c) Nonlinear LLE** **(d) Nonlinear t-SNE**

**Fig. 12 Results from dimensionality reduction of dynamic flap actuation.**

Finally, as in the prescribed pitching test presented in the previous section, we find similar patterns for the sinusoidal flap actuation in Figure 12. The t-SNE method, once again, fails to provide any substantial information on dominant structures in low dimensions. While being an efficient algorithm for classification tasks, the t-SNE is not suited for simulating dynamics. Another interesting observation is the similarity of the flap actuation kPCA manifold and that of the static aerodynamic test case shown in Figure 8b. It can be inferred that the effect of actuation of flap on pressure redistribution, in the presence of flow separation and shock, is limited. However, with flap actuation, we have lesser damping towards the attractor and this can be attributed to the excitation profile as before.

## V. Conclusions and Future Work

From the work presented here, the following major conclusions are drawn:

1) Patterns exist in the nonlinear flow field around an airfoil with shockwaves. These can be represented in terms of 2D or 3D manifolds. The benefits of this are two-fold. Firstly, the computational costs are minimised due to reduction of the system DOF by two orders of magnitude. Secondly, the system can be represented by 2 or 3

most dominant parameters in the latent manifold. This aids the physical intuition of the system properties and reduces the dependence on "hyper-parameters".

2) Certain machine learning tools such as kPCA and LLE have the potential to perform a meaningful transformation into the latent dimensions. It is imperative to relate these transformations to first principles such as stability theory and bifurcations in order to make data-driven predictions generalisable and interpretable.

Future work involves:

1) From preliminary tests conducted on performance of ANNs [data not shown], unsupervised algorithms such as kPCA and LLE are seen to identify the underlying dominant patterns while also minimising the error in reconstruction. Although ANNs are considered to be universal approximators, the high degree of variance in their architecture such as the need for training datasets, the number of hyperparameters, the number of sequential dense layers etc, results in the need to have specific constraints. Further evaluation of these autoencoders remains the subject of future work. Also, not all unsupervised algorithms pertaining to dimensionality reduction are suitable for a given task. The t-SNE algorithm was seen to perform a classification of the underlying dataset in most cases and is not suited for a pattern recognition task of a dynamical system.

2) Analyse the high-fidelity data from heave, pitch and flap simulations shown in this paper: The preliminary results generated for oscillatory input signals illustrate the existence of latent coordinates that have a parametric dependence on input frequency. This will be further extended to study the patterns obtained for varying frequencies.

3) Develop a physics-informed neural network: In the preliminary tests, neural networks were evaluated in a limited sense with a simple architecture. This will be extended to deep neural networks with sequential layers and physics information such as low-dimensional patterns and time integration module to obtain a Physics Informed Neural Network - Reduced Order Model (PINN-ROM). Future applications involve the use in a coupled aeroservoelastic environment. This is illustrated in Figure 13.

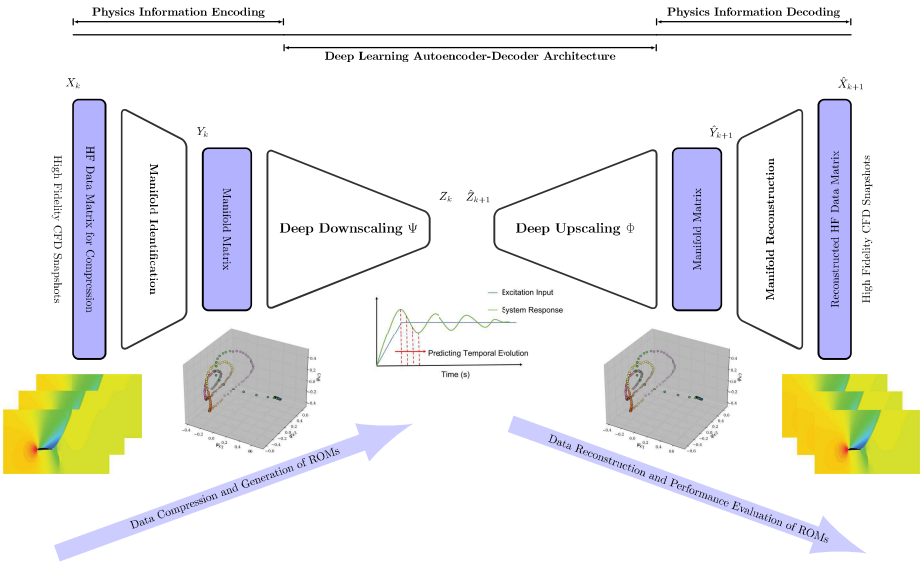


**Fig. 13 Illustration of the complete methodology for generating the PINN-ROM.**

## VI. Acknowledgements

The authors of this work would like to express their sincere gratitude to the Department of Aerospace Engineering at the Delft University of Technology for their support in sponsoring the Smart-Flying V project.

## References

[1] Wang, Y., Song, H., Pant, K., Brenner, M. J., and Suh, P. M., "Model order reduction of aeroservoelastic model of flexible aircraft," *57th AIAA/ASCE/AHS/ASC Structures, Structural Dynamics, and Materials Conference*, 2016, p. 1222.

[2] Ewins, D. J., *Modal testing: theory, practice and application*, John Wiley & Sons, 2009.

[3] Bui-Thanh, T., Damodaran, M., and Willcox, K., "Aerodynamic data reconstruction and inverse design using proper orthogonal decomposition," *AIAA journal*, Vol. 42, No. 8, 2004, pp. 1505–1516.

[4] Willcox, K., "Unsteady flow sensing and estimation via the gappy proper orthogonal decomposition," *Computers & fluids*, Vol. 35, No. 2, 2006, pp. 208–226.

[5] Benner, P., Gugercin, S., and Willcox, K., "A survey of projection-based model reduction methods for parametric dynamical systems," *SIAM review*, Vol. 57, No. 4, 2015, pp. 483–531.

[6] Opgenoord, M. M., Drela, M., and Willcox, K. E., "Physics-based low-order model for transonic flutter prediction," *AIAA Journal*, Vol. 56, No. 4, 2018, pp. 1519–1531.

[7] Fonzi, N., Brunton, S. L., and Fasel, U., "Data-driven nonlinear aeroelastic models of morphing wings for control," *Proceedings of the Royal Society A*, Vol. 476, No. 2239, 2020, p. 20200079.

[8] Brunton, B. W., Johnson, L. A., Ojemann, J. G., and Kutz, J. N., "Extracting spatial–temporal coherent patterns in large-scale neural recordings using dynamic mode decomposition," *Journal of neuroscience methods*, Vol. 258, 2016, pp. 1–15.

[9] Mendez, M. A., Hess, D., Watz, B. B., and Buchlin, J.-M., "Multiscale proper orthogonal decomposition (mPOD) of TR-PIV data—a case study on stationary and transient cylinder wake flows," *Measurement Science and Technology*, Vol. 31, No. 9, 2020, p. 094014.

[10] Brunton, S. L., and Kutz, J. N., *Data-Driven Science and Engineering: Machine Learning, Dynamical Systems, and Control*, 1st ed., Cambridge University Press, USA, 2019.

[11] Amsallem, D., and Farhat, C., "Interpolation method for adapting reduced-order models and application to aeroelasticity," *AIAA journal*, Vol. 46, No. 7, 2008, pp. 1803–1813.

[12] Washabaugh, K., Amsallem, D., Zahr, M., and Farhat, C., "Nonlinear Model Reduction for CFD Problems Using Local Reduced Order Bases," 2012. https://doi.org/10.2514/6.2012-2686.

[13] Carlberg, K., and Farhat, C., "An Adaptive POD-Krylov Reduced-Order Model for Structural Optimization," *8th World Congress on Structural and Multidisciplinary Optimization, Lisbon, Portugal*, 2009.

[14] Amsallem, D., Cortial, J., Carlberg, K., and Farhat, C., "A method for interpolating on manifolds structural dynamics reduced-order models," *International Journal for Numerical Methods in Engineering*, Vol. 80, No. 9, 2009, pp. 1241–1258.

[15] Brunton, S. L., Proctor, J. L., and Kutz, J. N., "Discovering governing equations from data by sparse identification of nonlinear dynamical systems," *Proceedings of the National Academy of Sciences*, Vol. 113, No. 15, 2016, pp. 3932–3937. https://doi.org/10.1073/pnas.1517384113, URL https://www.pnas.org/doi/abs/10.1073/pnas.1517384113.

[16] Lee, K., and Carlberg, K. T., "Model reduction of dynamical systems on nonlinear manifolds using deep convolutional autoencoders," *Journal of Computational Physics*, Vol. 404, 2020, p. 108973.

[17] Callaham, J. L., Brunton, S. L., and Loiseau, J.-C., "On the role of nonlinear correlations in reduced-order modelling," *Journal of Fluid Mechanics*, Vol. 938, 2022. https://doi.org/10.1017/jfm.2021.994, URL https://doi.org/10.1017%2Fjfm.2021.994.

[18] Deng, N., Noack, B. R., Morzyń ski, M., and Pastur, L. R., "Low-order model for successive bifurcations of the fluidic pinball," *Journal of Fluid Mechanics*, Vol. 884, 2019. https://doi.org/10.1017/jfm.2019.959, URL https://doi.org/10.1017%2Fjfm.2019.959.

[19] Mücke, N. T., Bohté, S. M., and Oosterlee, C. W., "Reduced Order Modeling for Parameterized Time-Dependent PDEs using Spatially and Memory Aware Deep Learning," *J. Comput. Sci.*, Vol. 53, 2021, p. 101408.

[20] Legaard, C. M., Schranz, T., Schweiger, G., Drgoňa, J., Falay, B., Gomes, C., Iosifidis, A., Abkar, M., and Larsen, P. G., "Constructing Neural Network-Based Models for Simulating Dynamical Systems," , 2021. https://doi.org/10.48550/ARXIV.2111.01495, URL https://arxiv.org/abs/2111.01495.

[21] Bertrand, X., Tost, F., and Champagneux, S., "Wing airfoil pressure calibration with deep learning," *AIAA Aviation 2019 Forum*, 2019, p. 3066.

[22] Rozov, V., and Breitsamter, C., "Data-driven prediction of unsteady pressure distributions based on deep learning," *Journal of Fluids and Structures*, Vol. 104, 2021, p. 103316. https://doi.org/https://doi.org/10.1016/j.jfluidstructs.2021.103316, URL https://www.sciencedirect.com/science/article/pii/S0889974621000992.

[23] Spalart, P., and Allmaras, S., "A one-equation turbulence model for aerodynamic flows," *30th aerospace sciences meeting and exhibit*, 1992, p. 439.

[24] Swischuk, R., Mainini, L., Peherstorfer, B., and Willcox, K., "Projection-based model reduction: Formulations for physics-based machine learning," *Computers & Fluids*, Vol. 179, 2019, pp. 704–717.

[25] Schölkopf, B., Smola, A., and Müller, K.-R., "Nonlinear component analysis as a kernel eigenvalue problem," *Neural computation*, Vol. 10, No. 5, 1998, pp. 1299–1319.

[26] Roweis, S. T., and Saul, L. K., "Nonlinear dimensionality reduction by locally linear embedding," *science*, Vol. 290, No. 5500, 2000, pp. 2323–2326.

[27] Jespersen, D. C., Pulliam, T. H., and Childs, M. L., "Overflow turbulence modeling resource validation results," Tech. rep., 2016.

[28] Coles, D., and Wadcock, A. J., "Flying-hot-wire study of flow past an NACA 4412 airfoil at maximum lift," *AIAA Journal*, Vol. 17, No. 4, 1979, pp. 321–329.